SSRG International Journal of Electronics and Communication Engineering
ISSN: 2348-8549/ https://doi.org/10.14445/23488549/IJECE-V11I4P110

Volume 11 Issue 4, 89-101, April 2024


*Original Article*

# Electromechanical Modelling and Analysis of RF MEMS Switch for mm-wave Application

R. Karthick[1], S.P.K. Babu[2]

[1]*Department of Physics, Periyar Maniammai Institute of Science and Technology (Deemed to be University), Tamilnadu, India.*
[2]*Department of Electronics and Communication Engineering, Periyar Maniammai Institute of Science and Technology (Deemed to be University), Tamilnadu, India.*

[1]*Corresponding Author : iamrkarthick85@gmail.com*

Received: 11 February 2024 Revised: 10 March 2024 Accepted: 09 April 2024 Published: 30 April 2024

***Abstract -*** *This paper presents the design, simulation, and analysis of two fundamental configurations aimed at implementing capacitive MEMS switches in a shunt arrangement. The objective of this systematic electromechanical modeling approach is to create MEMS switches with a low actuation voltage while preserving their RF and dynamic performance, especially for mm-wave applications. The switch's dynamic performance was analyzed utilizing COMSOL Multiphysics software, while the radio frequency (RF) properties were acquired through the employment of the HFSS software. The structure of Design 1, without flexure, results in a spring constant of 1.57 N/m and a resonant frequency of 54 kHz. Conversely, Design 2, incorporating a Fixed-Fixed flexure, demonstrates a spring constant of 0.80 N/m and a resonant frequency of 38 kHz, accomplished through meticulous adjustment of the thickness-to-length ratio. Both designs employ Aluminium as the material for the beam, with specifications of 260 µm for length, 100 µm for breadth, and 0.5 µm for thickness. Taking into account the influence of squeeze film, a finalized gap of 1.9 µm between the upper electrode and dielectric layer leads to a pull-in voltage of 7 V for Design 1 and 4.4 V for Design 2, respectively. A thorough investigation of incorporating 60 holes, each measuring 64 µm² (8µm x 8µm), in the beam membrane of Design 2 has been conducted. The inclusion of these holes reduces the pull-in voltage to 4 V and the switching time to 28 µs. Additionally, it effectively mitigates most of the stress experienced by the structure. Finally, the addition of a dielectric layer measuring 0.1 µm, utilizing $Si_3N_4$ as the dielectric material, further justifies the optimized structure of Design 2 as suitable for operating throughout the frequency range of 15 to 40 GHz*

***Keywords -*** *mm-wave, RF MEMS switch, Shunt capacitive switch, ICT, IoT.*

## 1. Introduction

The research community within electronics, Radio Frequency (RF) components/platforms, system integration and engineering, and Information and Communication Technology (ICT) has been significantly influenced by key drivers, encompassing the Internet of Things (IoT), Internet of Everything (IoE), Tactile Internet, and the advent of 5G in mobile communications [1, 2]. The 5G network is anticipated to accommodate various paradigms, ranging from widespread Machine-to-Machine (M2M) communications related to household and personal appliances to substantial multimedia data streams for Extended Reality (XR) [3, 4].

The ultimate goal is to achieve cities, industries, farms, and automobiles inside a fully interconnected and unified framework, which is more accurately described as the 5G ecosystem [5]. Given the necessitated capabilities of this communication standard, which include high data rates, expanded allocated spectrum, utilization of massive Multiple-Input-Multiple-Output (MIMO) systems, as well as beam steering and beam forming, the emphasis will be placed on devices such as switches, phase shifters, attenuators, filters, and their associated packaging and integration. Radio-Frequency Microelectromechanical Systems (RF MEMS) technology is increasingly recognized as a crucial facilitator for meeting the rigorous demands imposed by the evolving communication standards on passive devices and networks [6, 7]. These demands include high operating frequencies, extensive tunability, minimized hardware redundancy, and low power consumption [2, 8].

RF MEMS switches surpass traditional mechanical and semiconductor switches in the millimeter-wave frequency range, addressing various limitations and offering the additional advantage of functioning at elevated power levels [9]. While semiconductor switches exhibit faster switching times, smaller sizes, lower actuation voltages, and reduced losses, they face challenges in power handling capacity, power isolation, and insertion rate [10]. Switches are categorized as capacitive (metal-dielectric-metal) or ohmic (metal-metal)

based on electrode contact modes [10]. The resistive coupled ohmic contact type switch allows excessive current flow, resulting in a shortened switch lifespan, reduced reliability, and operational limitations within 15 GHz [11]. Although both contact types have similar power handling capabilities, capacitive contacts are preferred for high-frequency applications like 5G and prospective 6G applications due to their superior capacitance ratio between ON and OFF states [12].

The RF MEMS switch utilizes thermal, piezoelectric, electromagnetic, and electrostatic actuation mechanisms [13]. Despite the electrostatic mechanism requiring higher actuation voltages, it is widely employed due to its lower power consumption and favourable linearity [14]. Alternative actuation mechanisms suffer from increased power consumption and the inability to manage intricate circuits [15].

RF MEMS switches are further classified as series and shunt based on their beam configuration. A typical series switch configuration, employing a cantilever structure, achieves higher switching speeds and lower actuation voltages but is only suitable for lower frequencies. This is due to issues such as stiction, increased power consumption, self-latching from interfacial stress, and complex fabrication steps associated with open-contact transmission lines [16]. In contrast, the shunt arrangement with a fixed-fixed structure is better suited for high-frequency applications, offering stability, simpler fabrication, enhanced stress management capability, and fewer parasites in continuous transmission lines [17].

Many researchers have used various frameworks, materials, and strategies to optimise the performance of RF MEMS switches and make them more suitable for specific applications. A comprehensive evaluation of RF-MEMS switches used in 5G scenarios is carried out by [5], and the specific requirements needed for RF MEMS switches are described. The frequency range is as follows: low-frequency band: below 6 GHz; high-frequency band: between 24.25~27.5 GHz and 37~43.5 GHz for China; 27.5~28.28 GHz for Japan; 26.5~29.5 GHz for Korea; 27.5~28.35 GHz, 37~40 GHz and 64~71 GHz for the US; and 24.25~27.5 GHz for Europe.

Isolation is better than -30 / -40 dB at frequencies as high as possible. Expecting less than 1dB of insertion loss throughout the broadest frequency range; Switching time: lesser than one millisecond. Actuation voltage: between 2-3 volts; reliability or lifetime: over one billion ($10^9$) switching cycles; compatible with typical CMOS technology in terms of packaging and integration. Many switch designs and implementations for 5G applications are found in the literature.

In [6], the RF MEMS switch design operates at a central resonant frequency of 3.6 GHz and 3.4 GHz. This switch can be used in mobile communication devices and the design of 5G mobile network architecture, especially in the arrays of integrated antennas and radio-frequency interface modules. The shunt capacitive RF MEMS switch designed in [18] is in the frequency range of 24.25 GHz to 27.5 GHz (5G frequency band). At 26 GHz, the proposed switch reached an isolation of up to -41 dB, with a return loss below -14 dB and insertion loss below -0.20 dB.

In [19], a MEMS switch was designed specifically for millimetre wave 5G applications and needed an actuation voltage of 4.8 V. The mechanical resonant frequency, quality factor, and switching time were 8.35 kHz, 1.2, and 33 microseconds, respectively. In [20], a bridge-type RF MEMS switch was proposed for applications in 5G and 6G communications. Double-Diagonal (DDG) beam suspension with two or three anchoring points and a window was developed and optimised to minimise membrane deformation caused by residual stresses and coupling with the bottom electrode.

Section 2 of the manuscript outlines the operational mechanisms and configurations of design 1 and design 2 within the framework under investigation. In Section 3, an in-depth analysis of the theoretical underpinnings essential to switch design is provided. This examination encompasses key aspects, including pull-in voltage, switching time, capacitance analysis, and the methodology employed in material selection-subsequently, Section 4 proceeds to elucidate and analyse the results acquired from the simulation. Finally, Section 5 provides a summary of the study's findings and prospects for future exploration.

## 2. Working and Design

### *2.1. Working*

The switch configuration entails a shunt capacitive bridge characterized by a fixed-fixed beam structure, where the beam is designed to mimic two cantilevers arranged in a back-to-back configuration, as shown in Figure 1 [10].

Electrostatic actuation is employed to control the state of the switch. The thin metal beam is suspended over a coplanar waveguide (CPW), forming a bridge-like structure. In its initial or "upstate" position, the beam remains stiff, allowing the signal to flow through the CPW without hindrance [10].

This condition corresponds to the switch being in an ON state. To enhance the Radio Frequency (RF) performance of the switch, a thin layer of dielectric material is applied to the signal line of the coplanar waveguide. This dielectric layer serves the purpose of augmenting capacitance, thereby contributing to an improved performance of the switch in RF applications [21].

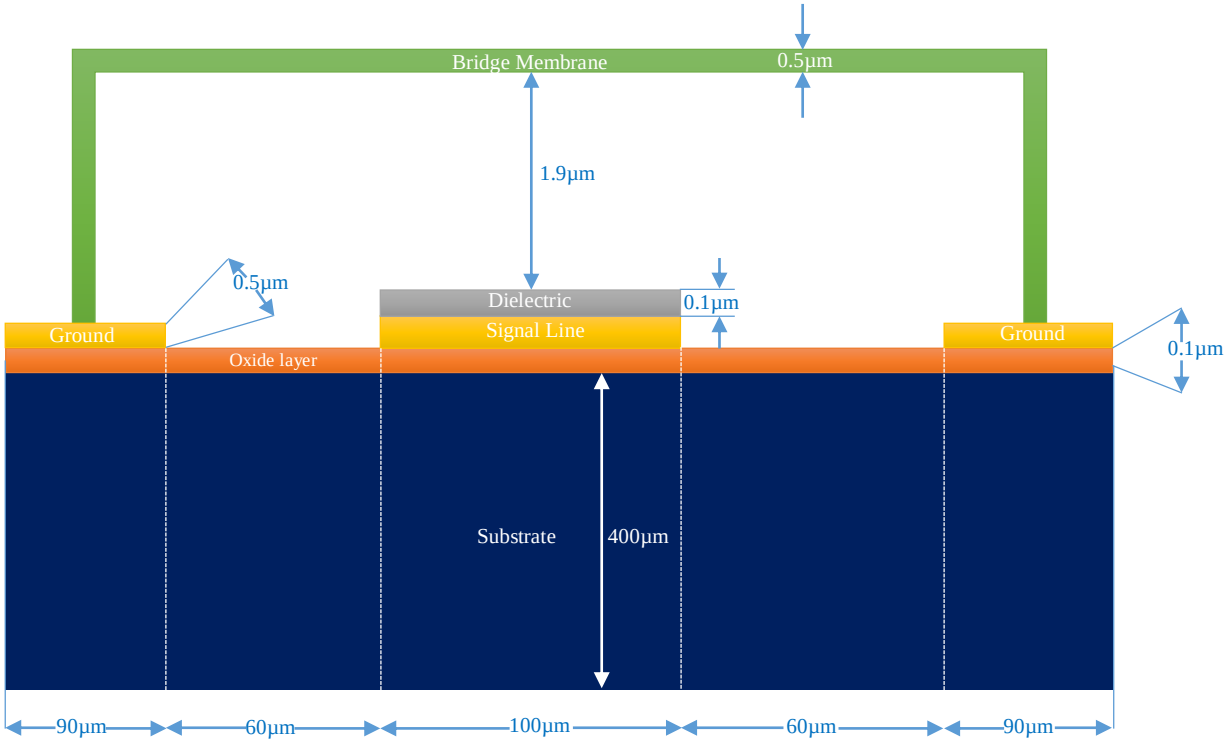


**Fig. 1 Cross-sectional view of capacitive shunt switch**

The specific selection of this design underscores its applicability to millimetre-wave (mm-wave) scenarios, emphasizing its suitability for high-frequency RF signals [22]. The beam is in its original position, and there is no contact between the signal line and the ground lines. When an actuation potential is applied across the beam, and the signal line, an electrostatic force of attraction is induced, pulling the beam downward. The mechanical stiffness of the beam structure counteracts the electrostatic force, maintaining balance. As the applied potential is increased, it reaches a point known as the pull-in voltage. At this voltage, the induced electrostatic force overcomes the mechanical restoring force of the beam [23].

The beam snaps down, making contact with the central signal line of the CPW (Coplanar Waveguide). This action terminates the signal flow in the central signal line, effectively putting the switch in the OFF state. The RF signal is then coupled to the ground lines. The switch is now considered actuated or in the OFF state, isolating the central signal line. When the applied actuation voltage is removed, the mechanical stiffness of the beam causes it to move back to its original position. The switch returns to its initial state, allowing the signal to flow through the central signal line again.

### *2.2. Design*

This study analyses two basic pre-existing geometric configurations. Design 1 represents a beam structure without meanders, as depicted in Figure 1. Similarly, Figure 2 illustrates the beam structure with fixed-fixed flexures, referred to as design 2. The spring constant is calculated using the formula illustrated in Equations 1 and 2.

For design 1,

$$k = 32Ew\left(\frac{t}{l}\right)^3 \quad (1)$$

For design 2,

$$k = 4Ew\left(\frac{t}{l}\right)^3 \quad (2)$$

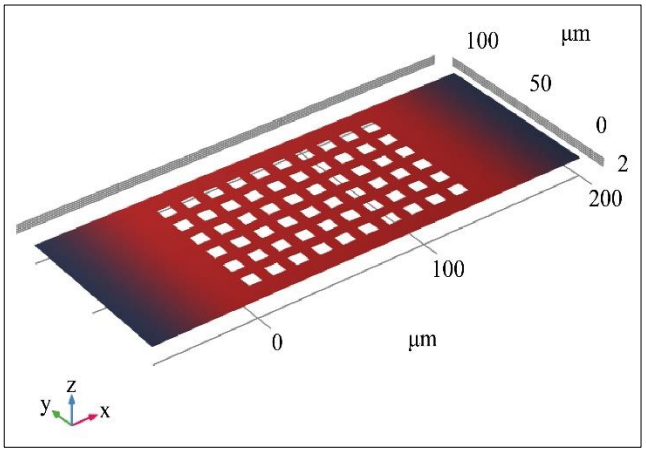


**Fig. 2 Beam structure of design 1**

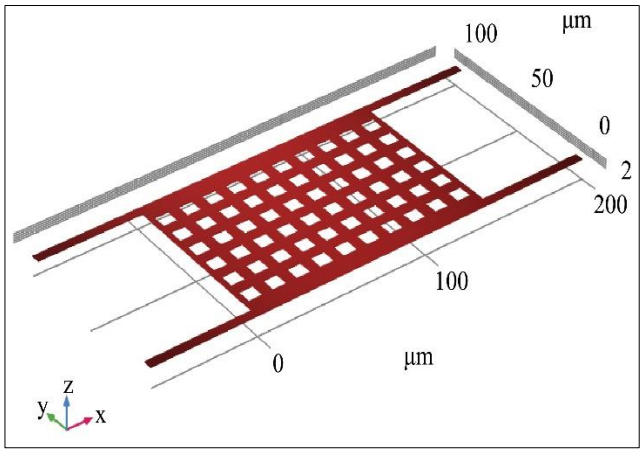


**Fig. 3 Beam structure of design 2**

Where $E$ stands for Young's modulus of the beam, $w$ is the width of the beam, $t$, and $l$ are the thickness and length of the beam, respectively [10].

## 3. Theoretical Analysis

### *3.1. Spring Constant and Pull-in Voltage*

The spring constant of the beam membrane plays a crucial role in the mechanical functioning of the RF MEMS switch. The structure's stiffness is determined by the spring constant of the fixed-fixed beam and quantifies the external force $F$ (N) required to induce small deflections $\Delta g$ (m) within the beam, as shown in Equation 3 [10].

$$F = k\Delta g \tag{3}$$

The effective spring constant of the beam dictates the pull-in voltage required for switching operations. The application of voltage between the bridge membrane and the bottom electrode generates electrostatic force within the beam. By treating the beam and lower electrodes as a parallel plate capacitor, the induced force can be calculated [24].

The electrostatic force (applied) $F_e$ necessary to bring the beam into the ON or OFF states is expressed as,

$$F_e = -\frac{\varepsilon_0 W_W V^2}{2g^2} \tag{4}$$

The stiffness-induced mechanical restoring force $F_r$ of the beam is expressed as,

$$F_r = k(g_0 - g) \tag{5}$$

Where, $g_0$ is the zero bias beam height.

The electrostatic force rises with the applied voltage as a result of charge accumulation, causing a decrease in the beam's height [25]. As the voltage is further increased, the beam becomes unstable at $2/3\ g_0$, where the increasing electrostatic force surpasses the restoring force. The pull-down voltage ($V_p$) is calculated as,

$$V_p = V(2g_0/3) = \sqrt{\frac{8k}{27\varepsilon_0 Ww}{g_0}^3} \tag{6}$$

The relationship described in Equation 6 indicates that $V_p$ is directly connected to both the spring constant ($k$) and the gap ($g_0$). If the values of $k$ and $g_0$are decreased, it will result in a corresponding drop in the pull-in voltage [26].

### *3.2. Switching and Release Time*

The switching time is characterized as the period required for the bridge membrane to move downward and reach the dielectric layer upon actuation. This time is dependent on the applied voltage, where a higher voltage results in a larger electrostatic force, consequently influencing the switching time. Equation 7 is utilized to calculate the switching time.

$$t_s = 3.67\frac{V_p}{V_s\,\omega_0} \tag{7}$$

Where, $V_s$ is the supply voltage and $\omega_0 (\omega_0 = \sqrt{k/m})$ is the resonant frequency of the resonant beam. It is evident from Equation 7 that the switching time decreases as the applied actuation voltage increases. Consequently, by applying $V_s$, which is 1.4 times higher than $V_p$, the time required to pull down the beam can be decreased [19].

When the switch is in an unactuated state, following the cessation of the actuation voltage, the duration it takes for the beam to traverse within 10% of the gap is denoted as the release time of the switch. The switch's release time is influenced by the mechanical restoring force, which functions to pull the beam back to its undeflected position.

$$t_r = \frac{\pi}{2}\sqrt{\frac{m}{k}} \tag{8}$$

According to Equation 8, the release time of the switch is inversely proportional to the spring constant of the beam structure. Therefore, to enhance the switch's release time, it is crucial to ensure that the beam possesses an appropriate spring constant [27].

### *3.3. Quality Factor Analysis and Holes in the Beam*

As these switches typically operate under atmospheric pressure, the activation of the MEMS beam involves collisions with the surrounding air and the electrode. This collision results in an increase in air viscosity, influencing key fluid mechanics factors such as the Knudsen number, squeeze number and damping coefficient. The Knudsen number represented in Equation 9 plays a role in determining the viscosity of the gas beneath the MEMS beam. The flow is less

viscous and there are few collisions when the Knudsen number is high [10].

$$K_n = \frac{\lambda}{g} \tag{9}$$

Where $\lambda$ defines the mean free path, which is the distance traveled by a molecule in a gas between consecutive collisions, the squeeze number depicted in Equation 10 is a parameter that characterizes how quickly the gas escapes from the gap during actuation. If the squeeze number ($\sigma \leq 3$) is low, the gas exits the gap without compression. Conversely, when the squeeze number is high, viscosity cause the gas to become trapped within the gap [28].

$$\sigma = \frac{12\mu_e l^2}{Pag^2}\omega \tag{10}$$

Where μ coefficient of viscosity of gas. For ideal gas like air at STP, viscosity is $1.854X\ 10^{-5} kg/ms$.

The primary concern with the squeeze number is that it contributes to an increase in the spring constant of the beam. The squeeze number may decrease with an increasing gap, but Knudsen's number decreases as well with an increasing gap. Thus, there is a trade-off between adjusting the gap to manage the squeeze number and maintaining an adequate Knudsen number [29].

Switching and settling time is directly proportional to the system's damping coefficient and quality factor. In MEMS switches, squeeze film damping has a significant impact on the quality factor [30].

A higher quality factor ($Q$) doesn't significantly impact the switching time but has a notable effect on the settling time. For switches with a quality factor less than 1, the switching time tends to be lower, while a $Q$ greater than 2 results in a higher settling time. Hence, it is advisable to maintain a value close to $Q \approx 1$.The quality factor is calculated as,

$$Q = \frac{k}{(\omega_0 b)} \tag{11}$$

Where, b - damping coefficient

It is suggested to introduce holes in the top membrane of the switch to maintain an appropriate damping coefficient, particularly for MEMS switches with lower heights [31]. The equation for the damping coefficient can be expressed as,

$$b = \frac{12}{N\pi}\frac{\mu A^2}{g_0^3}\left(\frac{P}{2} - \frac{P^2}{8} - \frac{\ln(p)}{4} - \frac{3}{8}\right) \tag{12}$$

Where $A$ is the area of the plate, $\mu$ is the coefficient of viscosity, $N$ is the total number of holes in the beam, and $P$ is the total area covered by the holes. Therefore, by introducing holes in the membrane with precise sizes and intervals, the switching dynamics of the device can be improved. Although introducing holes in the membrane can mitigate squeeze film damping, it is recommended to limit the number and coverage of holes to maintain the reliability and RF performance of the switch [20].

### *3.4. Capacitance and RF Performance Analysis*

A typical capacitive MEMS shunt switch resembles a parallel plate capacitor, where the thin beam switch membrane acts as the upper electrode, and the signal line of the Coplanar Waveguide (CPW) functions as the lower electrode [32].

The capacitance in the unactuated state of the switch is determined by the switch membrane while it is in its upstate position, representing the upstate capacitance. Conversely, the capacitance during the actuated state is influenced by the switch membrane in its downstate position, indicating the downstate capacitance of the switch.

An optimal shunt capacitive switch demonstrates effective isolation in the downstate and minimal insertion loss in the upstate position. The ratio between upstate and downstate capacitance determines the extent of both insertion and isolation loss [33].

The capacitance ratio between the upstate and the downstate can be expressed as,

$$C_r = \frac{C_d}{C_u} = \frac{\left(\frac{\varepsilon_0\,\varepsilon_r A}{t_d}\right)}{\left(\frac{\varepsilon_0\,A}{g+\frac{t_d}{\varepsilon_r}}\right)} \tag{13}$$

The impedance of a switch is represented through a CLR circuit, where the circuit parameters include variable capacitance($C = C_d + C_u$), inductance (L) and resistance (R).

$$Z_s = R_s + j\omega L + \frac{1}{j\omega C} \tag{14}$$

The impedance of a switch is influenced by its resonant frequency, as illustrated in Equation 15.

$$Z_s = \begin{cases} \frac{1}{j\omega C}, f \ll f_0 \\ R_s, f = f_0 \\ j\omega L, f \gg f_0 \end{cases} \tag{15}$$

The CLR circuit functions as a capacitor at frequencies below the resonant frequency and as an inductor at frequencies above it. Series resistance is introduced by CLR at the resonant frequency [34].

### *3.5. Material Selection for Beam and Dielectric*

The optimization of the physical properties and performance of a switch is subject to diverse constraints. The effectiveness of switch design is evident only when employing materials with characteristics that are well-suited for the intended purpose [35].

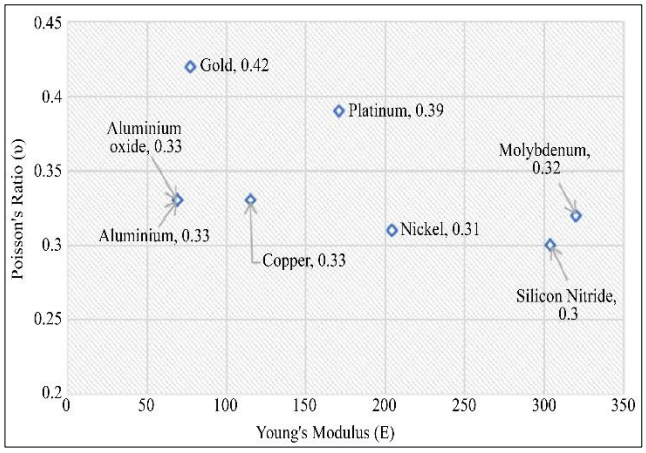


**Fig. 4 Material specifications of the beam membrane**

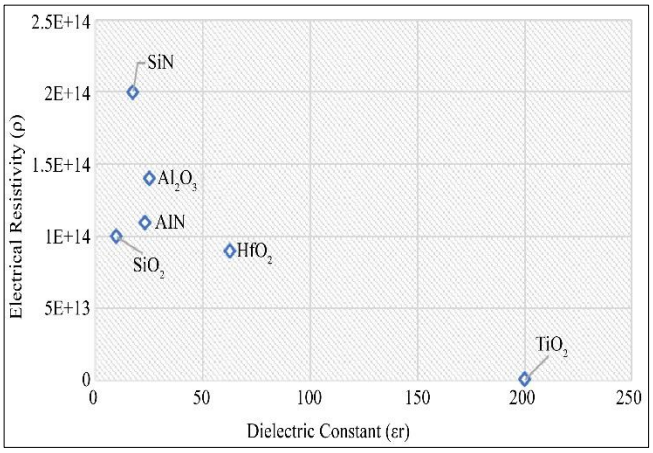


**Fig. 5 Material specifications of the dielectric layer**

Pull-in voltage can be decreased by selecting a material with a higher Poisson's ratio and thermal expansion coefficient. By employing materials that have lower electrical resistivity and Young's modulus values, RF losses may be minimized [36]. Materials exhibiting higher thermal conductivity and lower electrical resistivity result in minimal thermal residual stress. The graph depicted in Figure 4 demonstrates the characteristics of various materials suitable for beam membranes. Considering all these parameters, aluminum is determined to be the appropriate material for the design of the bridge membrane [37].

Selecting a dielectric material characterized by high electrical resistivity and dielectric constant contributes to an increased stiction relaxation time [38]. This, in turn, accelerates the decay of polarization, consequently diminishing the impact of dielectric charging. The use of a material with a higher dielectric constant lowers the hold-down voltage and augments the downstate capacitance, thereby enhancing the RF performance of the switch [39].

To achieve reasonable stability of the dielectric layer, it is crucial to select a material with a suitable Young's modulus value (neither too low nor too high), along with a lower Poisson's ratio and thermal expansion coefficient [40]. Figure 5 illustrates the properties of different materials appropriate for a dielectric layer.

## 4. Result and Discussion

### *4.1. Effect of Thickness-to-Length Ratio of the Beam*

#### *4.1.1. Spring Constant*

The spring constant can be characterized by the beam's Young's modulus, width, and thickness-to-length ratio, as depicted in Equations 1 and 2. The most suitable material for the design of the bridge membrane is aluminum, with a Young's Modulus ($E$) of 69 $GPa$, as elaborated in section 3.6. Altering the width of the beam is not advisable, as it could have an impact on the switch's RF functionality.

Hence, it is recommended to maintain a width within the range of 80 µm to 120µm. The intended spring constant may be achieved by experimenting with different $t/l$ ratios. Figure 6 illustrates the variation of the spring constant and stress for different thickness-to-length ($t/l$) ratios, considering a constant thickness of 0.5 µm. Similarly, Figure 7 depicts the changes in spring constant and stress for various $t/l$ ratios with a fixed length of 260 µm.

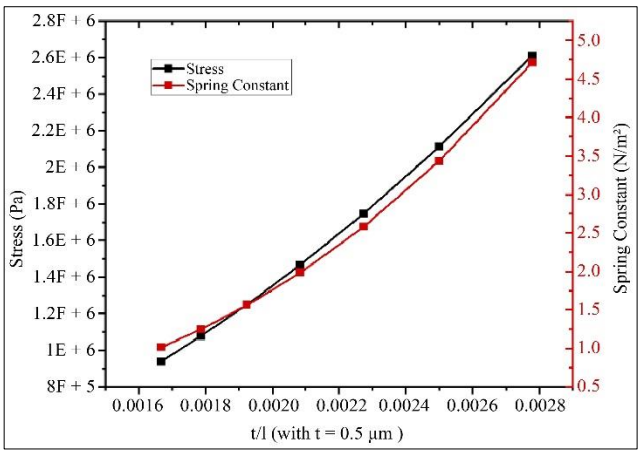


**Fig. 6 Stress and spring constant v/s ratio of thickness to length (with t=0.5 µm**

Figures 6 and 7 emphasise that maintaining a thickness-to-length ($t/l$) ratio within the range of 0.0015 to 0.0020 yields a better spring constant while keeping stress at an acceptable level. A shorter beam length can withstand more compressive stress, but it introduces a trade-off in the form of a significantly higher pull-down voltage. Hence, an optimal

configuration is identified with a beam thickness of 0.5 µm, a width of 100 µm, and a length of 260 µm for both design 1 and design 2.

Furthermore, design 2 of the switch incorporates specific meander structures to minimize the spring constant, consequently resulting in a reduction of the pull-in voltage. The spring constant for the beam structure in design 1 is determined to be 1.57 N/m. Conversely, in design 2, which incorporates a distinct meander, the effective spring constant is calculated to be 0.80 N/m.

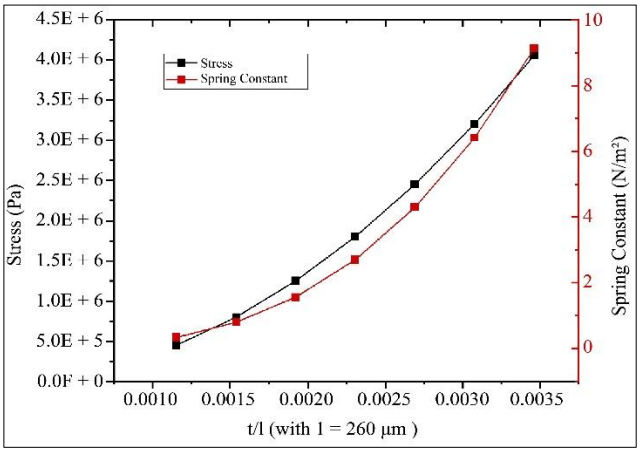


**Fig. 7 Stress and spring constant v/s ratio of thickness to length (with l=260 µm**

*4.1.2. Resonant Frequency*

The mechanical response of a switch under DC voltage is defined by its resonant frequency. This frequency, directly related to the square root of the spring's stiffness and the mass of the beam, holds significant importance in determining key switch characteristics such as switching time and quality factor.

The beam's mass, calculated as the product of the volume of the beam structure and the density of the chosen beam material, is determined to be 0.135 mg for Aluminum. Design 1 provides a resonant frequency of 54 kHz, while Design 2 offers a resonant frequency of 38 kHz.

### *4.2. Effect of Gap*

*4.2.1. Damping Coefficient and Pull-in Voltage*

As indicated by Equation 6, a practical method to decrease the pull-in voltage, apart from modifying the spring constant, involves adjusting the gap ($g_0$).

Expanding the area ($A$) of the beam membrane is not recommended, as it results in an enlargement of the overall switch size. Conversely, reducing the gap ($g_0$) between the lower electrode and the switch beam membrane has the potential to contribute to a reduction in the pull-in voltage.

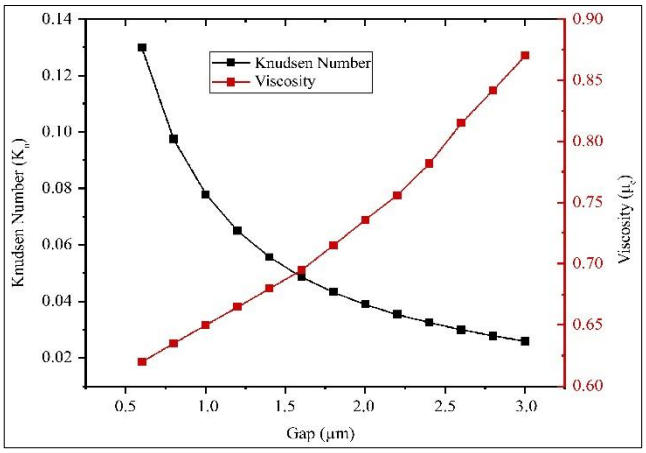


**Fig. 8 Knudsen number and viscosity v/s gap**

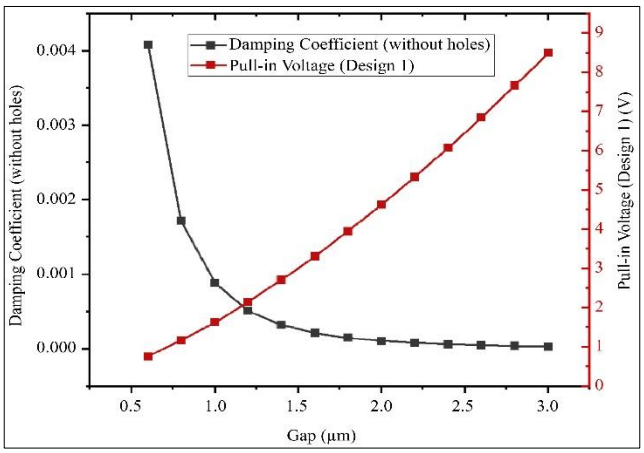


**Fig. 9 Damping coefficient and pull-in voltage v/s gap**

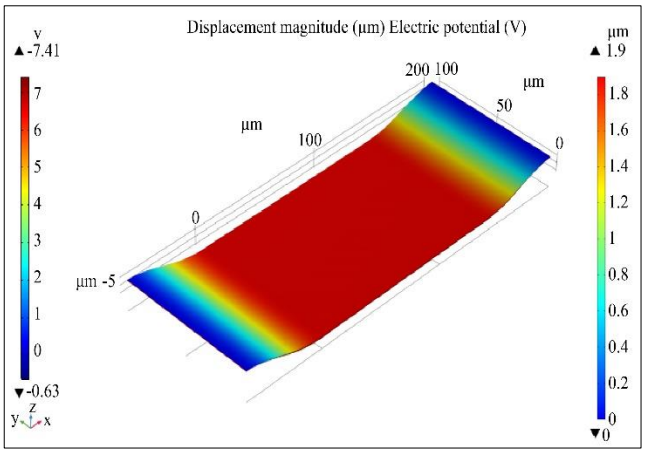


**Fig. 10 Displacement of beam membrane for design 1**

However, the theoretical examination presented in section 3.4 illustrates that reducing the gap forces the damping coefficient to increase and the Knudsen number to decrease, both of which are considered undesirable. Therefore, it is essential to maintain a gap that is neither too high nor too low between the bottom dielectric layer and the top beam structure.

Figure 8 graphically illustrates in variation of Knudsen number and Viscosity with respect to variation in Gap.

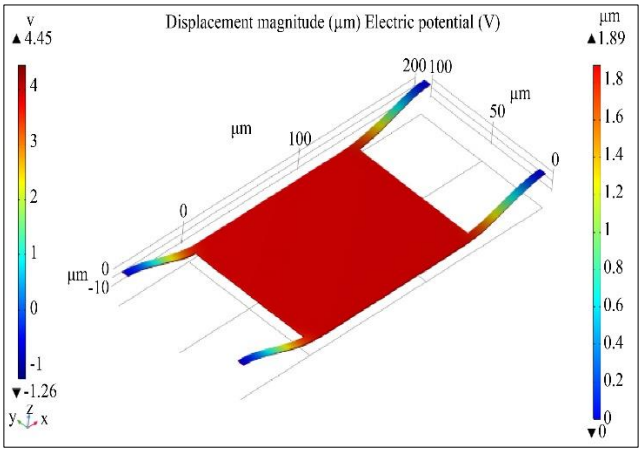


**Fig. 11 Displacement of beam membrane for design 2**

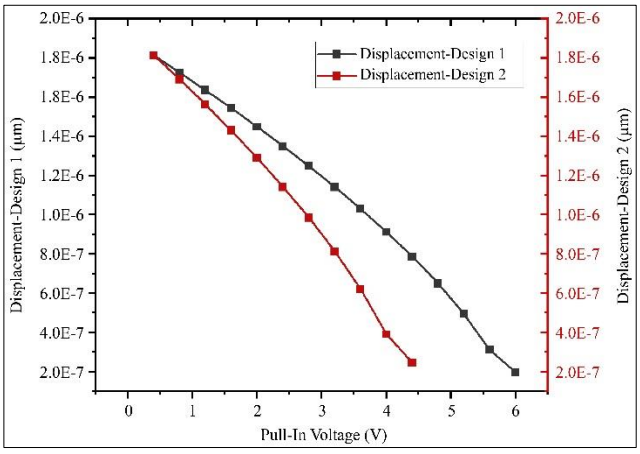


**Fig. 12 Pull-in voltage v/s displacement (design 1 and 2)**

Similarly, Figure 9 graphically depicts the variation of the damping coefficient and pull-in voltage in response to changes in gap ($g_0$). Both Design 1 and Design 2 are recommended with a 1.9 μm gap to enhance the damping coefficient while maintaining a lower pull-in voltage.

The switch membrane is designed and simulated using the FEM tool COMSOL Multiphysics (version 5.6), incorporating a spring constant of 1.57 $N/m$ for Design 1 and 0.08 $N/m$ for Design 2. Figures 10 and 11 visually represent the relationship between beam displacement and applied voltage for Design 1 and 2, respectively. Figure 12 provides a comparative analysis of the pull-in voltage for both designs, aiming to achieve a displacement of 1.9 $\mu m$.

### *4.3. Effect of Incorporating Holes*

*4.3.1. Quality Factor*

The switch's beam membrane is enhanced by incorporating an array of perforations, each measuring 64 μm² (8μm x 8μm), with the aim of improving switching dynamics and minimizing squeeze film damping. Table 1 delivers a thorough examination of diverse array sizes, revealing their respective quality factors.

The bold numbers in Table 1 indicate the recommended array of holes designed to enhance the quality factor ($Q\sim1$) for both Design 1 and Design 2.

**Table 1. Quality factor for different arrays of holes**

| Array of Holes | Damping Coefficient | Quality Factor | |
|---|---|---|---|
| | | Design 1 | Design 2 |
| 6 X 6 (36) | 3.267E-05 | 0.8 | 0.6 |
| 7 X 6 (42) | 2.707E-05 | **1.07** | 0.76 |
| 8 X 6 (48) | 2.297E-05 | 1.26 | 0.88 |
| 9 X 6 (54) | 1.986E-05 | 1.46 | **1.04** |
| 10 X 6 (60) | 1.743E-05 | 1.66 | **1.18** |
| 11 X 6 (66) | 1.547E-05 | 1.87 | 1.3 |

*4.3.2. Pull-in Voltage*

An array of 60 holes, each with a size of 64 μm², is integrated into the beam of Design 1. To achieve a displacement of 1.9 μm, the beam's pull-in voltage must be 4.4 V without any holes and 4 V with holes, as illustrated in Figures 11 and 13, respectively.

*4.3.3. Stress Analysis*

A Von Mises stress analysis is conducted for the beam structure of Design 1 with holes. In Figure 14, the beam structure without holes experiences a maximum stress of 77.5 MPa, while the beam structure with holes, shown in Figure 15, encounters a reduced maximum stress of only 37.6 MPa.

Therefore, the presence of holes' aids in releasing Von Mises stress around them without compromising the reliability of the switch.

*4.3.4. Switching Time*

An RF MEMS switch's switching time can be characterized as the duration it takes for the bridge membrane to descend and make contact with the dielectric layer when a pull-in voltage is applied.

Analyzing the switching behavior of the beam membrane, this study compares the membrane with holes and without holes for Design 2. Figure 16 visually presents the results of this investigation.

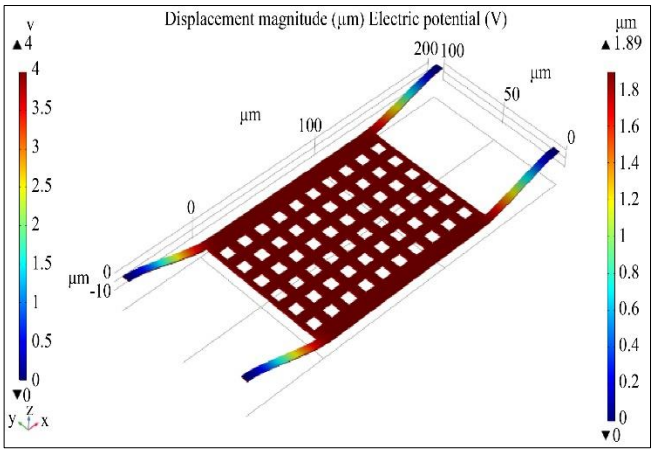


**Fig. 13 Displacement of beam membrane with holes for design 2**

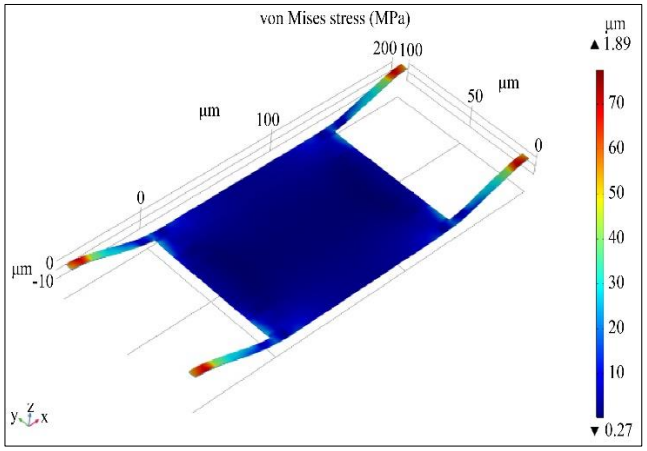


**Fig. 14 Von mises stress analysis of the beam membrane without holes for design 2**

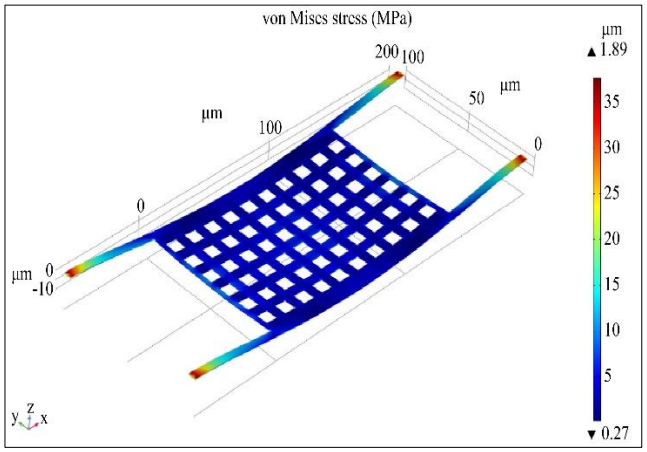


**Fig. 15 Von mises stress analysis of the beam membrane with holes for design 2**

### *4.4. Effect of Dielectric Layer*

Dielectric materials with different thicknesses are employed in MEMS switches between the bottom electrode and the beam. Equation 13 implies that considering the impact of dielectric thickness and its relative dielectric constant is essential, as these factors become inevitable when calculating the capacitance of a MEMS switch. Enhancing radio frequency performance necessitates raising the capacitance ratio, which may be accomplished by laying a thin dielectric layer with a high dielectric constant.

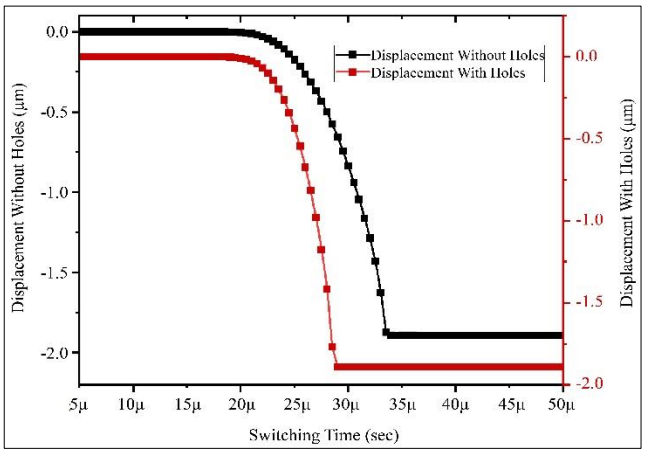


**Fig. 16 Switching analysis of the beam membrane with holes and without holes for design 2**

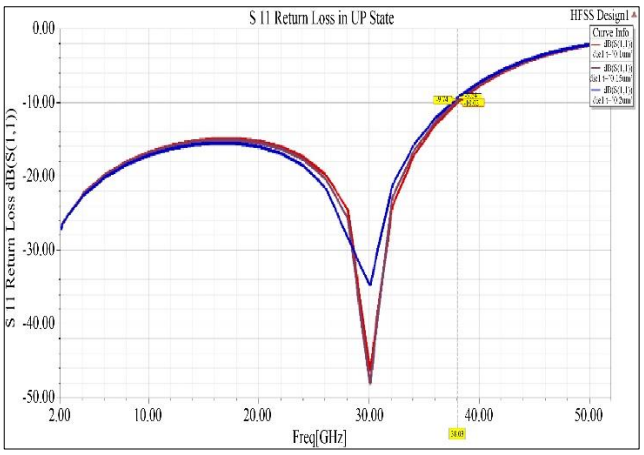


**Fig. 17 Return loss in the upstate for different dielectric thickness**

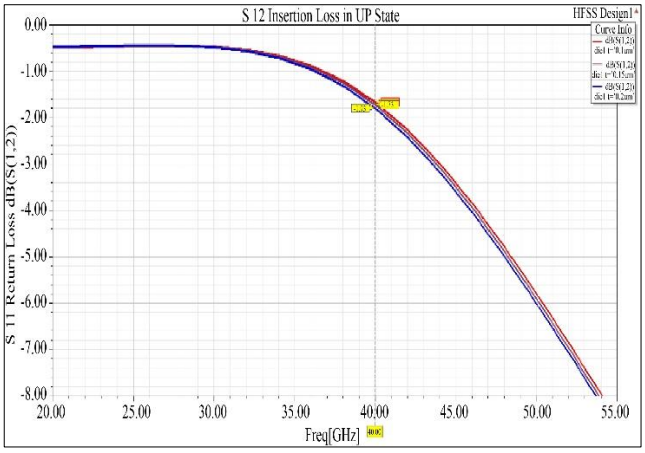


**Fig. 18 Insertion loss in the upstate for different dielectric thickness**

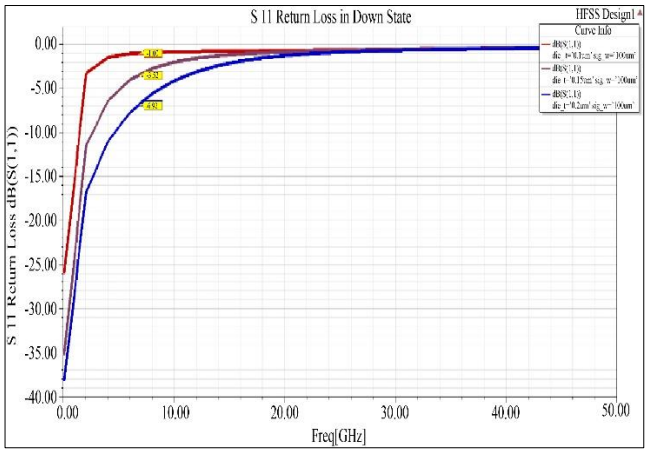


**Fig. 19 Return loss in downstate for different dielectric thickness**

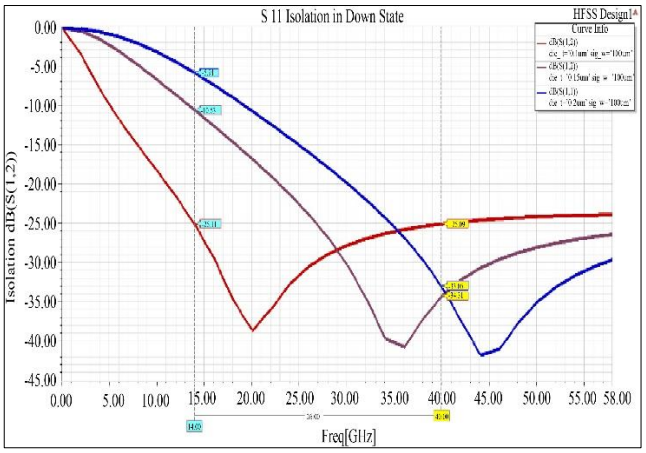


**Fig. 20 Isolation in downstate for different dielectric thickness**

**Table 2. Comparison of proposed work with existing literature**

| Parameters | [19] | [41] | [42] | This Work [Design 2] |
|---|---|---|---|---|
| Membrane Thickness (µm) | 0.5 | 1 | 1.2 | 0.5 |
| Air Gap (µm) | 2 | 3 | 1 | 1.9 |
| Dielectric Layer Thickness (µm) | 0.15 | 0.20 | 0.10 | 0.10 |
| Frequency Range (KHz) | 20-40 | 38 | 4-26 | 14-40 |
| Pull-in-Voltage(V) | 4.80 | 11.97 | 18 | 4 |
| Capacitance Ratio | 0.08pF/0.69pF | 31fF/0.152pF | 20 | 210 |
| Quality Factor | 1.2 | - | - | 1.18 |
| Switching Speed (µSec) | 33 | 190 | - | 28 |
| Insertion Loss (dB) | −0.6dB for 20-40GHz | < 1dB @ 38GHz | -0.65dB @ 24GHz | -1dB @ 40GHz |
| Return Loss (dB) | Less than 12dB for 20-40GHz | -13dB @ 38GHz | -22 dB @ 24GHz | -46dB @ 38GHz |
| Isolation (dB) | >40dB for 20-40 GHz | -31dB @ 38GHz | -18dB @ 24GHz | -25dB from 14GHz – 40 GHz |

Nevertheless, difficulties like pinhole formation and manufacturing complexity make it challenging to adhere to a dielectric layer thinner than 1000 Å. Figures 17 and 18 illustrate the return loss and insertion loss in the "Up" state for various dielectric thicknesses. Similarly, the isolation and return loss in the "Down" state are shown in Figures 19 and 20 for different dielectric thicknesses.

### *4.5. Comparison with Existing Research*

The results obtained in this work are compared with the existing works available in the literature. The comparison is given in Table 2. The parameters taken for comparison cover the entire details of the switch where our research shows better performance in pull-in voltage, Quality factor, Capacitance ratio and operating frequency range. It is also found that the parameters such as return loss and isolation in downstate can be improved.

## 5. Conclusion

This paper discusses the design, simulation, and analysis of capacitive shunt MEMS switches in two different configurations. Aluminium is chosen as the material for the beam, and physical optimization is conducted to improve the spring constant, resulting in a beam structure with dimensions of 260 µm in length, 100 µm in width, and 0.5 µm in thickness. This optimization yields a spring constant of 1.57 N/m and a resonant frequency of 54 kHz for Design 1 and a spring constant of 0.80 N/m with a resonant frequency of 38 kHz for

Design 2. When analysing the Pull-in voltage requirement for an optimized gap of 1.9 µm, Design 2 outperforms Design 1 by requiring a pull-in voltage of 4.4 V, whereas Design 1 requires 7V. In order to enhance the switching dynamics, 60 holes are introduced into the beam membrane, each measuring 64 µm² in size. Analysis of the dynamic behavior using COMSOL Multiphysics software on Design 2, with the incorporation of these holes, demonstrates that a significant portion of the stress is dissipated through the holes.

As a result, the pull-in voltage is reduced to 4V, and the switch time is reduced to 28 µs. By employing $Si_3N_4$ as the dielectric material with a thickness of 0.1 µm, the radio frequency (RF) characteristics are assessed using HFSS software. The analysis validates that the optimized structure of Design 2 is well-suited for operation within the frequency range of 15 to 40 GHz.

In future iterations, refining the optimized design to achieve lower pull-in voltage and enhanced switching time would be advantageous. Introducing serpentine meanders into the structure represents a promising avenue for improvement. This modification holds the potential for fine-tuning the performance characteristics of the MEMS switches.

## Acknowledgments

We express our gratitude for the software support received from the I-STEM program, funded by the Office of the Principal Scientific Adviser to the Government of India, which generously provided the COMSOL Multiphysics FEM software (Version 5.6) to facilitate our research efforts.The authors would like to thank Dr. Raghuraman Selvaraju, RF Application Engineer & Business Development Executive, Elmack Engg. Services Pvt. Ltd for providing valuable suggestions in improving the RF performance.

## References

[1] Jacopo Iannacci, and H. Vincent Poor, "Review and Perspectives of Micro/Nano Technologies as Key-Enablers of 6G," *IEEE Access*, vol. 10, pp. 55428-55458, 2022. [CrossRef] [Google Scholar] [Publisher Link]

[2] Xiaohu You et al., "Towards 6G Wireless Communication Networks: Vision, Enabling Technologies, and New Paradigm Shifts," *Science China Information Sciences*, vol. 64, pp. 1-74, 2021. [CrossRef] [Google Scholar] [Publisher Link]

[3] David Dubuc, Katia Grenier, and Jacopo Iannacci, *18 - RF-MEMS for Smart Communication Systems and Future 5G Applications*, Smart Sensors and MEMs, 2nd ed., pp. 499-539, 2018. [CrossRef] [Google Scholar] [Publisher Link]

[4] Chuan Zhang et al., "Artificial Intelligence for 5G and Beyond 5G: Implementations, Algorithms, and Optimizations," *IEEE Journal on Emerging and Selected Topics in Circuits and Systems*, vol. 10, no. 2, pp. 149-163, 2020. [CrossRef] [Google Scholar] [Publisher Link]

[5] Li-Ya Ma et al., "Comprehensive Study on RF-MEMS Switches Used for 5G Scenario," *IEEE Access*, vol. 7, pp. 107506-107522, 2019. [CrossRef] [Google Scholar] [Publisher Link]

[6] Alexey Tkachenko, Igor Lysenko, and Andrey Kovalev, "Investigation and Research of High-Performance RF MEMS Switches for Use in the 5G RF Front-End Modules," *Micromachines*, vol. 14, no. 2, pp. 1-42, 2023. [CrossRef] [Google Scholar] [Publisher Link]

[7] Raji George, C.R.S. Kumar, and S.A. Gangal, "Design of Series RF MEMS Switches Suitable for Reconfigurable Antenna Applications," *2017 International Conference on Circuit, Power and Computing Technologies (ICCPCT)*, Kollam, India, pp. 1-5, 2017. [CrossRef] [Google Scholar] [Publisher Link]

[8] Raj Kumari, and Mahesh Angira, "RF-MEMS Capacitive Switches: Enabling Transition Towards 5G/B5G Applications," *International Journal of Information Technology*, vol. 15, no. 7, pp. 3889-3897, 2023. [CrossRef] [Google Scholar] [Publisher Link]

[9] Vijay K. Varadan, K. J. Vinoy, and K. A. Jose, *RF MEMS and Their Applications*, Wiley, pp. 376, 2003. [Google Scholar] [Publisher Link]

[10] Gabriel M. Rebeiz, *RF MEMS: Theory, Design, and Technology*, Wiley, 2003. [CrossRef] [Google Scholar] [Publisher Link]

[11] Anurag Swarnkar, Amitava DasGupta, and Deleep R Nair, "Design, Fabrication and Characterization of RF MEMS Shunt Switch for Wideband Operation of 3 GHz to 30 GHz," *Journal of Micromechanics and Microengineering*, vol. 29, no. 11, 2019. [CrossRef] [Google Scholar] [Publisher Link]

[12] Isibor E. Obuh et al., "Low-Cost Microfabrication for MEMS Switches and Varactors," *IEEE Transactions on Components, Packaging and Manufacturing Technology*, vol. 8, no. 9, pp. 1702-1710, 2018. [CrossRef] [Google Scholar] [Publisher Link]

[13] Elham Pirmoradi, Hadi Mirzajani, and Habib Badri Ghavifekr, "Design and Simulation of a Novel Electro-Thermally Actuated Lateral RF MEMS Latching Switch for Low Power Applications," *Microsystem Technologies*, vol. 21, pp. 465-475, 2015. [CrossRef] [Google Scholar] [Publisher Link]

[14] Sai Pranav Chokkara et al., "Design, Simulation and Analysis of a Slotted RF MEMS Switch," *Transactions on Electrical and Electronic Materials*, vol. 23, pp. 419-429, 2022. [CrossRef] [Google Scholar] [Publisher Link]

[15] Li-Feng Wang et al., "Laterally-Actuated Inside-Driven RF MEMS Switches Fabricated by a SOG Process," *Journal of Micromechanics and Microengineering*, vol. 25, no. 6, 2015. [CrossRef] [Google Scholar] [Publisher Link]

[16] Qiannan Wu et al., "Design and Fabrication of a Series Contact RF MEMS Switch with a Novel Top Electrode," *Nanotechnology and Precision Engineering*, vol. 6, no. 1, 2023. [CrossRef] [Google Scholar] [Publisher Link]

[17] B.V.S. Sailaja, and Ketavath Kumar Naik, "Design and Analysis of Serpentine Meander Asymmetric Cantilever RF-MEMS Shunt Capacitive Switch," *Analog Integrated Circuits and Signal Processing*, vol. 102, pp. 593-603, 2020. [CrossRef] [Google Scholar] [Publisher Link]

[18] Vivek Verma, and Mahesh Angira, "A Shunt Capacitive Switch Based on RF MEMS Technology for 5G Application: Design and Investigation," *2021 International Conference on Intelligent Technologies (CONIT)*, Hubli, India, pp. 1-4, 2021. [CrossRef] [Google Scholar] [Publisher Link]

[19] Sudhanshu Shekhar, K J Vinoy, and G K Ananthasuresh, "Low-Voltage High-Reliability MEMS Switch for Millimeter Wave 5G Applications," *Journal of Micromechanics and Microengineering*, vol. 28, no. 7, 2018. [CrossRef] [Google Scholar] [Publisher Link]

[20] Jasmina Casals-Terré et al., "Enhanced Robustness of a Bridge-Type Rf-Mems Switch for Enabling Applications in 5G and 6G Communications," *Sensors*, vol. 22, no. 22, pp. 1-20, 2022. [CrossRef] [Google Scholar] [Publisher Link]

[21] Vishram B. Sawant, Suhas S. Mohite, and Laukik N. Cheulkar, "Comprehensive Contact Material Selection Approach for RF MEMS Switch," *Materialstoday Proceedings*, vol. 5, no. 4, pp. 10704-10711, 2018. [CrossRef] [Google Scholar] [Publisher Link]

[22] Osor Pertin, and Kurmendra, "Pull-in-Voltage and RF Analysis of MEMS Based High Performance Capacitive Shunt Switch," *Microelectronics Journal*, vol. 77, pp. 5-15, 2018. [CrossRef] [Google Scholar] [Publisher Link]

[23] Afshin Kashani Ilkhechi et al., "A New Electrostatically Actuated Rotary Three-State DC-Contact RF MEMS Switch for Antenna Switch Applications," *Microsystem Technologies*, vol. 23, pp. 231-243, 2017. [CrossRef] [Google Scholar] [Publisher Link]

[24] Tai-Ran Hsu, *MEMS and Microsystems: Design and Manufacture*, McGraw Hill, pp. 1-436, 2002. [Google Scholar] [Publisher Link]

[25] W. Merlijn Van Spengen, Robert Puers, and Ingrid De Wolf, "On the Physics of Stiction and its Impact on the Reliability of Microstructures," *Journal of Adhesion Science and Technology*, vol. 17, no. 4, pp. 563-582, 2003. [CrossRef] [Google Scholar] [Publisher Link]

[26] G.M. Rebeiz, and J.B. Muldavin, "RF MEMS Switches and Switch Circuits," *IEEE Microwave Magazine*, vol. 2, no. 4, pp. 59-71, 2001. [CrossRef] [Google Scholar] [Publisher Link]

[27] Kurmendra, and Rajesh Kumar, "A Review on RF Micro-Electro-Mechanical-Systems (MEMS) Switch for Radio Frequency Applications," *Microsystem Technologies*, vol. 27, no. 7, pp. 2525-2542, 2021. [CrossRef] [Google Scholar] [Publisher Link]

[28] Sudhanshu Shekhar, K.J. Vinoy, and G.K. Ananthasuresh, "Surface-Micromachined Capacitive RF Switches with Low Actuation Voltage and Steady Contact," *Journal of Microelectromechanical Systems*, vol. 26, no. 3, pp. 643-652, 2017. [CrossRef] [Google Scholar] [Publisher Link]

[29] Shankar Dutta et al., "Effect of Residual Stress on RF MEMS Switch," *Microsystem Technologies*, vol. 17, pp. 1739-1745, 2011. [CrossRef] [Google Scholar] [Publisher Link]

[30] Surendra K. Waghmare, and D.D. Shah, "RF MEMS Capacitive Shunt Switch : A Study Based Practical Overview," *International Journal of Applied Engineering Research*, vol. 13, no. 15, pp. 11830-11838, 2018. [Google Scholar] [Publisher Link]

[31] K. Guha et al., "Novel Analytical Model for Optimizing the Pull-in Voltage in a Flexured MEMS Switch Incorporating Beam Perforation Effect," *Solid-State Electronics*, vol. 137, pp. 85-94, 2017. [CrossRef] [Google Scholar] [Publisher Link]

[32] Hao Wei et al., "High On/Off Capacitance Ratio RF MEMS Capacitive Switches," *Journal of Micromechanics and Microengineering*, vol. 27, no. 5, 2017. [CrossRef] [Google Scholar] [Publisher Link]

[33] Kurmendra, and Rajesh Kumar, "A Modified Capacitance Model of Shunt Micro Switch Based on MEMS Technology in Actuation Mode: Simulation and Analytical Study," *Journal of Physics: Conference Series*, vol. 1432, no. 1, 2020. [CrossRef] [Google Scholar] [Publisher Link]

[34] J.B. Muldavin, and G.M. Rebeiz, "High-Isolation CPW MEMS Shunt Switches. 1. Modeling," *IEEE Transactions on Microwave Theory and Techniques*, vol. 48, no. 6, pp. 1045-1052, 2000. [CrossRef] [Google Scholar] [Publisher Link]

[35] Kurmendra, and Rajesh Kumar, "Materials Selection Approaches and Fabrication Methods in RF MEMS Switches," *Journal of Electronic Materials*, vol. 50, no. 6, pp. 3149-3168, 2021. [CrossRef] [Google Scholar] [Publisher Link]

[36] Julien G. Noel, "Review of the Properties of Gold Material for MEMS Membrane Applications," *IET Circuits, Devices and Systems*, vol. 10, no. 2, pp. 156-161, 2016. [CrossRef] [Google Scholar] [Publisher Link]

[37] M.F. Ashby et al., "Selection Strategies for Materials and Processes," *Materials & Design*, vol. 25, no. 1, pp. 51-67, 2004. [CrossRef] [Google Scholar] [Publisher Link]

[38] Kurmendra, and Rajesh Kumar, "Dielectric Material Selection for High Capacitance Ratio and Low Loss in MEMS Capacitive Switch Using Ashby's Methodology," *IOP Conference Series: Materials Science and Engineering*, vol. 1020, no. 1, 2021. [CrossRef] [Google Scholar] [Publisher Link]

[39] A. Basu, G.G. Adams, and N.E. McGruer, "A Review of Micro-Contact Physics, Materials, and Failure Mechanisms in Direct-Contact RF MEMS Switches," *Journal of Micromechanics and Microengineering*, vol. 26, no. 10, 2016. [CrossRef] [Google Scholar] [Publisher Link]

[40] Kurmendra, and Rajesh Kumar, "Investigations on Beam Membrane and Dielectric Materials Using Ashby's Methodology and their Impact on the Performance of a MEMS Capacitive Switch," *Microsystem Technologies*, vol. 27, no. 12, pp. 4269-4289, 2021. [CrossRef] [Google Scholar] [Publisher Link]

[41] K. Srinivasa Rao, P. Naveena, and K. Girija Sravani, "Materials Impact on the Performance Analysis and Optimization of RF MEMS Switch for 5G Reconfigurable Antenna," *Transactions on Electrical and Electronic Materials*, vol. 20, pp. 315-327, 2019. [CrossRef] [Google Scholar] [Publisher Link]

[42] Yasser Mafinejad, Hamid Reza Ansari, and Saeed Khosroabadi, "Development and Optimization of RF MEMS Switch," *Microsystem Technologies*, vol. 26, pp. 1253-1263, 2020. [CrossRef] [Google Scholar] [Publisher Link]